Analytic Solutions of Simple Flows and Analysis of Nonslip Boundary Conditions for the Lattice Boltzmann BGK Model

Xiaoyi He,[1,2] **Qisu Zou,**[1,3,5] **Li-Shi Luo,**[3,4,6] **and Micah Dembo**[2]

In this paper we analytically solve the velocity of the lattice Boltzmann BGK equation (LBGK) for several simple flows. The analysis provides a framework to theoretically analyze various boundary conditions. In particular, the analysis is used to derive the slip velocities generated by various schemes for the nonslip boundary condition. We find that the slip velocity is zero as long as $\sum_\alpha f_\alpha e_\alpha = 0$ at boundaries, no matter what combination of distributions is chosen. The schemes proposed by Noble *et al.* and by Inamuro *et al.* yield the correct zero-slip velocity, while some other schemes, such as the bounce-back scheme and the equilibrium distribution scheme, would inevitably generate a nonzero slip velocity. The bounce-back scheme with the wall located halfway between a flow node and a bounce-back node is also studied for the simple flows considered and is shown to produce results of second-order accuracy. The momentum exchange at boundaries seems to be highly related to the slip velocity at boundaries. To be specific, the slip velocity is zero only when the momentum dissipated by boundaries is equal to the stress provided by fluids.

---

[1] Center for Nonlinear Studies (CNLS), MS-B258, Los Alamos National Laboratory, Los Alamos, New Mexico 87545.
[2] Theoretical Biology and Biophysics Group (T-10), MS-K710, Theoretical Division, Los Alamos National Laboratory, Los Alamos, New Mexico 87545.
[3] Complex Systems Group (T-13), MS-B213, Theoretical Division, Los Alamos National Laboratory, Los Alamos, New Mexico 87545.
[4] Computational Science Methods Group (XCM), MS-F645, X Division, Los Alamos National Laboratory, Los Alamos, New Mexico 87545.
[5] Department of Mathematics, Kansas State University, Manhattan, Kansas 66506.
[6] ICASE, Mail Stop 403, NASA Langley Research Center, Hampton, Virginia 23681.

1. INTRODUCTION

In recent years, the lattice Boltzmann equation (LBE)[4–8] has been success-fully applied to various hydrodynamic problems which are difficult for con-ventional numerical methods (e.g., finite-difference or finite-element scheme). Among these problems are multiphase, multicomponent flows,[9, 10] magneto-hydrodynamics,[11] and reactive flows.[12] From a computational viewpoint, the notable advantages of the LBE method are parallelism of algorithm, sim-plicity of programming, and ease of incorporating microscopic interactions.

Although it has been proved[6, 7, 13] that the LBE recovers the Navier–Stokes equation with a second order of accuracy in space in the interior of flow domain, the real hydrodynamic boundary conditions have not been fully understood. For a node near a boundary, some of its neighboring nodes may locate outside the flow domain. The distribution functions from these nonfluid nodes are therefore unknown after each streaming process. The boundary condition is responsible for determining these unknown distributions.

In general, there are two ways to define a boundary: placing the boundary on grid nodes[1–3, 14] or placing the boundary on links.[10, 15, 16] No matter which method is used, to find out whether a boundary condition is appropriate, one would like to know the slip velocity introduced by the boundary condition. Many of the previous studies on the velocity bound-ary condition are based on numerical experiments. In ref. 14 the distribu-tion at a boundary node is set to the equilibrium distribution plus a modification term based the Chapman–Enskog expansion, and the velocity gradient in the modification is approximated by a finite difference. In ref. 1 the unknown distributions and density at a boundary node are obtained from the known distributions and the known velocities at the boundary for the triangular lattice. In refs. 2 and 3 the unknown distributions and density at a boundary node are obtained from the known distributions and the known velocities at the boundary with some additional assumptions of the unknown distributions. With numerical experiments, one can only observe the order of the slip velocity. How this slip velocity is generated and what factors it depends on are not well known. Hence, an analytical study is necessary for a better understanding of the model and the non-slip boundary condition on stationary or moving walls.

Some theoretical studies have been carried out on the LGA or the LBE model and the non-slip boundary condition on a stationary wall was studied.[15–18] The discussion in refs. 15 and 17 is based on a linearized lattice Boltzmann equation with a global equilibrium with constant density and isotropic velocity (zero velocity). In ref. 16 the boundary condition of the 3D FCHC lattice Boltzmann model[19, 20] with a linear collision

operator represented by a collision matrix A was studied for the plane Poiseuille flow and the plane stagnation flow. In that study, the first-order and second-order deviations of the distribution function from equilibrium were assumed to take an *a priori* form in terms of flow quantities. In ref. 18 analytical solutions of the distribution functions for Poiseuille flow and Couette flows were found for the FHP or the square LBGK models without any approximation. The study was restricted to situations that the velocity profile extends beyond the boundary in a smooth way and to the Poiseuille flow with square forcing given in ref. 21 for the FHP model. Nevertheless, all the previous theoretical studies only treated bounceback boundary conditions. The present study directly solves the LBGK equation without any approximations and hence it can handle various boundary conditions.

The paper is organized as follows. Section 2 analytically solves the nine-bit lattice Boltzmann BGK equation for the two-dimensional Poiseuille flow and the Couette flow with possible vertical injection at the boundaries. The results are further used to analyze different schemes for the non-slip boundary condition. Section 3 discusses the results and concludes the paper. The Appendix briefly discusses some results of the seven-bit (FHP) LBGK model.

2. ANALYTICAL SOLUTION AND NONSLIP BOUNDARY CONDITION

In this section, we use the square nine-bit lattice LBGK model. The procedure can be easily applied to the FHP model and some results are given in the Appendix. The nine-bit lattice BGK model is on a square lattice space with three speeds: 0, c, and $\sqrt{2}c$, where $c = \delta_x/\delta_t$, and δ_x and δ_t are the lattice constant and the step size in time, respectively. Figure 1 shows all possible velocities of the model. With the presence of a body force $\mathbf{F}$, the evolution equation of the system is

$$f_\alpha(\mathbf{x} + \mathbf{e}_\alpha \delta_t, t + \delta_t) - f_\alpha(\mathbf{x}, t) = -\frac{1}{\tau}[f_\alpha(\mathbf{x}, t) - f_\alpha^{(eq)}(\rho, \mathbf{u})] + \frac{\delta_t^2}{\delta_x} g_\alpha \quad (1)$$

where τ is the dimensionless relaxation time, and

$$\mathbf{e}_\alpha = \begin{cases} (0, 0), & \alpha = 0 \\ (\cos[(\alpha - 1)\,\pi/2], \sin[(\alpha - 1)\,\pi/2])\,c & \alpha = 1, 2, 3, 4 \\ (\cos[(\alpha - 5)\,\pi/2 + \pi/4], \sin[(\alpha - 5)\,\pi/2 + \pi/4])\,\sqrt{2}c & \alpha = 5, 6, 7, 8 \end{cases}$$
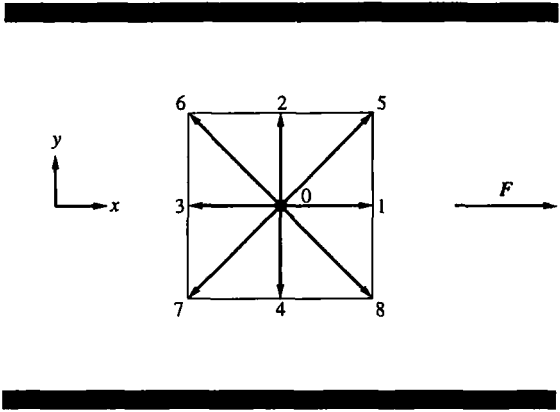
$$(2)$$

Fig. 1. All possible velocities for the nine-bit lattice BGK model on a square lattice. This figure also shows the arrangement for the channel flow and the Couette flow in simulations.

are the velocity vectors. The equilibrium distribution function $f_\alpha^{(eq)}(\rho, \mathbf{u})$ is given by

$$f_\alpha^{(eq)}(\rho, \mathbf{u}) = w_\alpha \rho \left[1 + 3 \left(\frac{\mathbf{e}_\alpha \cdot \mathbf{u}}{c^2} \right) + \frac{9}{2} \left(\frac{\mathbf{e}_\alpha \cdot \mathbf{u}}{c^2} \right)^2 - \frac{3}{2} \left(\frac{\mathbf{u}}{c} \right)^2 \right] \tag{3}$$

where $w_0 = 4/9$, $w_{1,2,3,4} = 1/9$, and $w_{5,6,7,8} = 1/36$. The local density of mass ρ and the local density of momentum $\rho\mathbf{u}$ in Eq. (3) are given by

$$\rho = \sum_\alpha f_\alpha \tag{4a}$$

$$\rho\mathbf{u} = \sum_\alpha \mathbf{e}_\alpha f_\alpha \tag{4b}$$

Finally, the forcing term g_α is given by

$$g_\alpha = \begin{cases} 0, & \alpha = 0 \\ \dfrac{1}{3c}\, \mathbf{e}_\alpha \cdot \mathbf{F}, & \alpha = 1, 2, 3, 4 \\ \dfrac{1}{12c}\, \mathbf{e}_\alpha \cdot \mathbf{F}, & \alpha = 5, 6, 7, 8 \end{cases} \tag{5}$$

The evolution of the lattice BGK system consists of two steps: collision and advection. First the distribution functions f_α at the site $\mathbf{x}$ undergo

the collision process, prescribed by the right of Eq. (1) or otherwise. After the collision, f_α moves to the next site, $\mathbf{x} + \mathbf{e}_\alpha \delta_t$, according to the velocity $\mathbf{e}_\alpha$.

The Navier–Stoke equation can be derived from Eq. (1):

$$\rho \frac{\partial \mathbf{u}}{\partial t} + \rho \mathbf{u} \cdot \nabla \mathbf{u} = -\nabla(c_x^2 \rho) + \nu \rho \nabla^2 \mathbf{u} + \mathbf{F} \tag{6}$$

where the kinetic viscosity is

$$\nu = \frac{(2\tau - 1)}{6} \frac{\delta_x^2}{\delta_t}$$

and the speed of sound is

$$c_x = \frac{1}{\sqrt{3}} c$$

In the following analysis, we will only consider steady (time-independent) flows satisfying

$$\frac{\partial u}{\partial x} = 0, \qquad \frac{\partial v}{\partial x} = 0, \qquad \rho = \text{const} \tag{7}$$

The body force is assumed to be along the x direction, i.e., $\mathbf{F} = \rho G \mathbf{i}_x$. In this type of flow, both the velocity and the distribution functions are only functions of the y coordinate. Although being rather simple, they serve as examples for us to carry out some theoretical analyses which can be further used to study the nonslip boundary condition.

By substituting Eqs. (3) and (7) into Eq. (1), we obtain the following equations:

$$f_0^j = \frac{4\rho}{9} \left[1 - \frac{3}{2} \left(\frac{u_j^2}{c^2} + \frac{v_j^2}{c^2} \right) \right] \tag{8a}$$

$$f_1^j = \frac{\rho}{9} \left[1 + 3 \frac{u_j}{c} + 3 \frac{u_j^2}{c^2} - \frac{3}{2} \frac{v_j^2}{c^2} \right] + \frac{\delta_x \tau \rho G}{3c^2} \tag{8b}$$

$$f_2^j = \frac{\rho}{9\tau} \left[1 + 3 \frac{v_{j-1}}{c} + 3 \frac{v_{j-1}^2}{c^2} - \frac{3}{2} \frac{u_{j-1}^2}{c^2} \right] + \frac{\tau - 1}{\tau} f_2^{j-1} \tag{8c}$$

$$f_3^j = \frac{\rho}{9} \left[1 - 3 \frac{u_j}{c} + 3 \frac{u_j^2}{c^2} - \frac{3}{2} \frac{v_j^2}{c^2} \right] - \frac{\delta_x \tau \rho G}{3c^2} \tag{8d}$$

$$f_4^j = \frac{\rho}{9\tau}\left[1 - 3\frac{v_{j+1}}{c} + 3\frac{v_{j+1}^2}{c^2} - \frac{3}{2}\frac{u_{j+1}^2}{c^2}\right] + \frac{\tau-1}{\tau}f_4^{j+1} \tag{8e}$$

$$f_5^j = \frac{\rho}{36\tau}\left[1 + 3\frac{u_{j-1}}{c} + 3\frac{v_{j-1}}{c} + 3\frac{u_{j-1}^2}{c^2} + 3\frac{v_{j-1}^2}{c^2} + 9\frac{u_{j-1}v_{j-1}}{c^2}\right]$$

$$+ \frac{\tau-1}{\tau}f_5^{j-1} + \frac{\delta_x\rho G}{12c^2} \tag{8f}$$

$$f_6^j = \frac{\rho}{36\tau}\left[1 - 3\frac{u_{j-1}}{c} + 3\frac{v_{j-1}}{c} + 3\frac{u_{j-1}^2}{c^2} + 3\frac{v_{j-1}^2}{c^2} - 9\frac{u_{j-1}v_{j-1}}{c^2}\right]$$

$$+ \frac{\tau-1}{\tau}f_6^{j-1} - \frac{\delta_x\rho G}{12c^2} \tag{8g}$$

$$f_7^j = \frac{\rho}{36\tau}\left[1 - 3\frac{u_{j+1}}{c} - 3\frac{v_{j+1}}{c} + 3\frac{u_{j+1}^2}{c^2} + 3\frac{v_{j+1}^2}{c^2} + 9\frac{u_{j+1}v_{j+1}}{c^2}\right]$$

$$+ \frac{\tau-1}{\tau}f_7^{j+1} - \frac{\delta_x\rho G}{12c^2} \tag{8h}$$

$$f_8^j = \frac{\rho}{36\tau}\left[1 + 3\frac{u_{j+1}}{c} - 3\frac{v_{j+1}}{c} + 3\frac{u_{j+1}^2}{c^2} + 3\frac{v_{j+1}^2}{c^2} - 9\frac{u_{j+1}v_{j+1}}{c^2}\right]$$

$$+ \frac{\tau-1}{\tau}f_8^{j+1} + \frac{\delta_x\rho G}{12c^2} \tag{8i}$$

where f_α^j is the distribution function and (u_j, v_j) is the velocity vector at $y = j\delta_x$. Equations (8) are valid for $2 \leqslant j \leqslant n-2$. The node $j = 0$ or $j = n$ corresponds to lower or upper boundaries, respectively, where the evolution rule depends on the implementation of boundary conditions.

In the interior of the flow domain ($2 \leqslant j \leqslant n-2$), the x component of the momentum density ρu_j can be rewritten as

$$\rho u_j = c[(f_1^j - f_3^j) + (f_5^j - f_6^j) + (f_8^j - f_7^j)]$$

$$= \frac{\tau+1}{3\tau}\rho u_j + \frac{2\tau-1}{6\tau}\rho(u_{j-1} + u_{j+1})$$

$$+ \frac{\rho}{2c\tau}(u_{j-1}v_{j-1} - u_{j+1}v_{j+1}) + \frac{\delta_t}{\tau}\rho G \tag{9}$$

which further gives us

$$\frac{u_{j+1}v_{j+1} - u_{j-1}v_{j-1}}{2\delta_x} = v\frac{u_{j+1} + u_{j-1} - 2u_j}{\delta_x^2} + G \tag{10}$$

The above equation is exactly the second-order finite-difference form of the simplified incompressible Navier–Stokes equation under the assumption (7) and constant pressure:

$$\frac{\partial(uv)}{\partial y} = v\frac{\partial^2 u}{\partial y^2} + G \tag{11}$$

In the y direction, from $\rho v_j = c[f_2^j - f_4^j + f_5^j + f_6^j - f_7^j - f_8^j]$, it is easy to prove

$$v_{j+1}^2 - v_{j-1}^2 = (2\tau - 1)(v_{j+1} + v_{j-1} - 2v_j)\,c \tag{12}$$

On the other hand, from $\rho = \sum_{i=0}^{8} f_i^j$ and the definition of ρv_j above, we can prove

$$v_{j+1}^2 + v_{j-1}^2 - 2v_j^2 = (2\tau - 1)(v_{j+1} - v_{j-1})\,c \tag{13}$$

Combination of Eqs. (12) and (13) yields

$$v_j = v_c = \text{const} \tag{14}$$

It should be noted that this result is only valid in the interior of the flow domain. Whether v_c is equal to the vertical velocity at boundaries v_b depends on the implementation of the boundary condition.

2.1. Poiseuille Flow

For the Poiseuille flow, the vertical velocity is zero and Eq. (10) has a simple solution:

$$u_j = \frac{4U_c}{n^2}j(n-j) + U_s, \qquad j = 1,\dots,n-1 \tag{15}$$

where $U_c = L^2 G/8v$ is the centerline velocity without slips at boundaries, with $L = n\delta_x$ being the width of the channel and U_s is the slip velocity depending on the implementation of the boundary condition for walls in a particular scheme. The above velocity profile is a parabola with a shift on the boundaries. The slip velocity U_s is the only term which makes the

solution of the LBGK possibly different from the exact solution of the Poiseuille flow.

In order to find the slip velocity, we need to apply Eq. (9) at the grid line next to the bottom wall ($j = 1$) (analysis for the top boundary is the same):

$$\rho u_1 = c[(f_1^1 - f_3^1) + (f_5^1 - f_6^1) + (f_8^1 - f_7^1)]$$

$$= \frac{\tau + 1}{3\tau} \rho u_1 + \frac{2\tau - 1}{6\tau} \rho(u_0 + u_2) + \frac{\delta_t}{\tau} \rho G + \left(1 - \frac{1}{\tau}\right) \rho(\tilde{u}_0 - u_0) \qquad (16)$$

which further yields

$$u_1 = \frac{u_0 + u_2}{2} + \frac{\delta_x^2}{2\nu} G + \frac{3(\tau - 1)}{2\tau - 1} [\tilde{u}_0 - u_0] \qquad (17)$$

In the derivation, it is assumed that $f_1^0, f_3^0, f_7^0, f_8^0$ follow the rules in Eqs. (8), the equilibrium distribution at $j = 0$ is calculated using velocity $(u_0, 0)$, and $\rho \tilde{u}_0 = c[(f_1^0 - f_3^0) + (f_5^0 - f_6^0) + (f_8^0 - f_7^0)]$, where f_5^0, f_6^0 depend on the boundary condition implemented. Comparing Eqs. (15) and (17), we obtain the explicit expression for the slip velocity:

$$U_s = \frac{6(\tau - 1)}{2\tau - 1} [\tilde{u}_0 - u_0] \qquad (18)$$

With this result, we can easily analyze different schemes for the nonslip boundary condition (u_0 is set to be zero in what follows for the sake of simplicity).

1. *Bounce-back scheme.* For the bounce-back scheme, the particle colliding with the wall simply reverses the direction of its velocity, that is,

$$f_2^1 = f_4^0, \qquad f_5^1 = f_7^0, \qquad f_6^1 = f_8^0 \qquad (19)$$

Notice that the collision process does not occur at the boundary in this scheme, hence Eq. (18) does not apply. Using the bounce-back rule, we can derive

$$U_s = \frac{2U_c}{3n^2} [(2\tau - 1)(4\tau - 3) - 3n] \qquad (20)$$

Clearly, the bounce-back rule generally yields a nonzero slip velocity. Furthermore, the slip velocity is of the first order in space because it has a term of $O(1/n)$.

2. *Modified bounce-back scheme.* By the modified bounce-back rule, we mean that collision and forcing still occur at boundary nodes. The precollision unknown distribution is set equal to the value of the distribution along the opposite direction:

$$f_2^0 = f_4^0, \qquad f_5^0 = f_7^0, \qquad f_6^0 = f_8^0 \tag{21}$$

With the modified bounce-back rule, we can prove

$$U_s = \frac{16\tau(\tau - 1)}{3n^2} U_c \tag{22}$$

Clearly, the modified bounce-back boundary condition also generate a nonzero slip velocity as long as $\tau \neq 1$. However, compared to the bounce-back rule, the error is reduced and the slip velocity is of the second order in space.

3. *Nonslip schemes.* In the nonslip scheme proposed by Noble et al.[2] the unknown distributions and the boundary density are calculated from the constraints given in Eq. (4) and an additional constraint given by

$$2\rho\varepsilon = \sum_\alpha (e_\alpha - u)^2 f_\alpha \tag{23}$$

where ε is the internal energy, which equals the square of the sound speed in the limit of low Mach number and low Knudsen number. In the nonslip scheme proposed by Inamuro et al.[3] it is assumed that the distributions at a horizontal boundary can be written in the following equilibrium form:

$$f_\alpha^0 = f_\alpha^{(eq)}(\rho', \mathbf{u}_w') \tag{24}$$

where $f_\alpha^{(eq)}$ is defined in Eq. (3) and $\mathbf{u}_w' = (u_0 + u', v_0)$. The two parameters ρ', u' and the density at the boundary are determined from the constraints (4).

From their definitions, it is easy to see both schemes lead to

$$\tilde{u}_0 = c[(f_1^0 - f_3^0) + (f_5^0 - f_6^0) + (f_8^0 - f_7^0)] = 0 \tag{25}$$

Therefore, the slip velocity is automatically zero and the nonslip boundary condition is implemented correctly. Notice that the distribution functions are different in these two schemes, and they are different from the analytical solution in ref. 18, but all three distribution functions give the correct velocity profile. In fact, any scheme which uses the known $f_1^0, f_3^0, f_4^0, f_7^0, f_8^0$

to generate f_2^0, f_5^0, f_6^0 according to $\sum_\alpha f_\alpha e_\alpha = 0$ and ensures the correct p will give the correct velocity profile for the Poiseuille flow. For example, we have obtained the boundary density from a consistency condition in Eq. (3) as in refs. 2 and 3 and have set $f_2^0 = p/\beta$ with β being an adjustable parameter, and the numerical simulations yielded the correct density and velocity profile of the Poiseuille flow for β varying from 0.01 to 10^8.

To verify our theoretical analysis, we have further carried out numerical simulations for the Poiseuille flow. Figure 2 shows the velocity profiles u_j normalized by U_c for the Poiseuille flow. The system size is $N_x \times N_y = 16 \times 4$. The amplitude of the uniform forcing along the x axis is 0.1. The density of the system is set to be 1.0. The initial state of the system is $u = 0$ and $v = 0$. The u_j are measured at a cross section of the channel after 5000 times iteration. Shown in Fig. 2 are the velocity profiles with different values of τ and with different implementations of the boundary condition for a stationary wall, i.e., the bounce-back rule, the modified bounce-back rule, and the nonslip boundary conditions in refs. 2 and 3. The result with the nonslip boundary condition is a perfect parabola without any slip velocity at the walls, while the results with the bounce-back or the modified bounce-back boundary condition have a nonzero slip velocity at the boundaries. Also, the numerical results are in excellent agreement with our
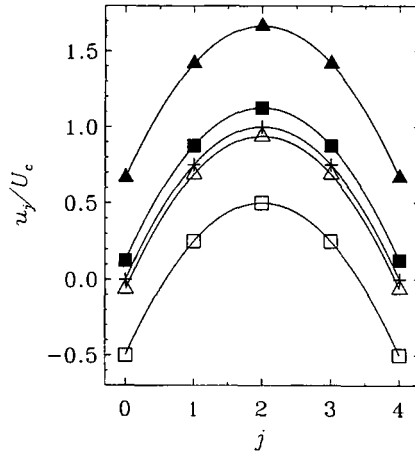

Fig. 2. The normalized velocity profile of the Poiseuille flow. Solid lines, our analytic results with various types of boundary conditions and values of τ. (+) The numerical results of lattice BGK simulation with the scheme in refs. 2 and 3; (■, □) the numerical results of lattice BGK simulation with the bounce-back boundary conditions; (▲, △) the results with the modified bounce-back boundary condition. The solid and open symbols represent the numerical results with $\tau = 2.0$ and 0.75, respectively.
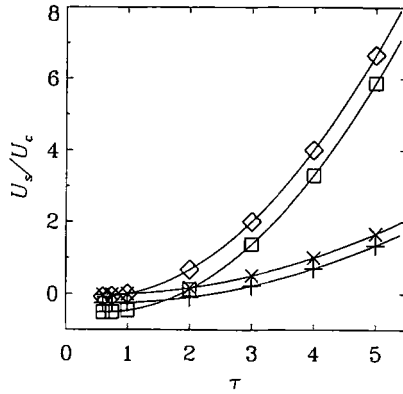
Fig. 3. The normalized slip velocity of the Poiseuille flow as a function of τ and the number of nodes across the channel, n, with two types of boundary conditions. Solid lines, our analytic results. ($\square$, $+$) The numerical results by the lattice BGK simulation with the bounce-back boundary condition and with $n = 4$ and 8, respectively; ($\diamond$, $\times$) the numerical results with the modified bounce-back boundary condition and with $n = 4$ and 8, respectively.

theoretical analysis. The error in the numerical results of u_j/U_c is of the order of 10^{-10}, which is of the order of the roundoff error.

Figure 3 shows the slip velocity U_s, normalized by U_c, as a function of τ and n for the Poiseuille flow with the bounce-back boundary condition. The analytic results are given by Eq. (20). We chose $n = 4$ and 8 in the simulations. The results of the simulations coincide perfectly with the analytic results.

2.2. Plane Couette Flow with Possible Injection at Boundaries

For the Couette flow with possible vertical injection at the boundaries, the body force G is zero. The lower and upper walls move along the horizontal direction at different velocities u_0 and u_n, respectively. In the mean time, a vertical velocity is injected at a speed of v_b at both walls. Equation (10) can be solved in the interior of the flow domain. Through some simple algebraic derivations we find

$$u_j = \frac{\lambda^j - 1}{\lambda^n - 1}\,(u_n + U_s^n) + \frac{\lambda^n - \lambda^j}{\lambda^n - 1}\,(u_0 + U_s^0) \tag{26}$$

We have $\lambda = (2 + R)/(2 - R)$, where $R = v_c \delta_x/\nu$, with v_c being the vertical velocity in the interior of the flow channel. The U_s^n and U_s^0 stand for the slip velocities at the top and bottom walls, respectively. Once the slip

velocities are set to zero, it is easy to prove that this solution is a second-order approximation of the analytical solution:

$$u = \frac{e^{Re \cdot y/L} - 1}{e^{Re} - 1} u_n + \frac{e^{Re} - e^{Re \cdot y/L}}{e^{Re} - 1} u_0 \tag{27}$$

where the Reynolds number $Re = v_b L/\nu$, with L being the width of the flow region. Note that with Re in Eq. (27) replaced by $Re^* = n \ln(\lambda)$, Eq. (26) differs from the analytical solution only by the slip velocities at the boundaries. The difference between Re and Re^* reflects the finite-difference errors and it vanishes when δ_x/L tends to zero.

Again, the slip velocities depend on how the boundary condition is implemented. Following the same procedure in deriving Eq. (10), we have the following recurrence relationships for the velocity near the bottom wall:

$$\frac{u_2 v_2 - u_0 v_0}{2\delta} = \nu \frac{u_2 + u_0 - 2u_1}{\delta^2} + \frac{\tau - 1}{\delta} [\tilde{u}_0 - u_0] \tag{28}$$

$$v_1^2 - v_0^2 = (2\tau - 1)(v_0 - v_1) c + 2(\tau - 1)(\tilde{v}_0 - v_0) c \tag{29}$$

where

$$\tilde{u}_0 = c[(f_1^0 - f_3^0) + (f_5^0 - f_6^0) + (f_8^0 - f_7^0)]$$

$$\tilde{v}_0 = c[(f_2^0 - f_4^0) + (f_5^0 + f_6^0) - (f_7^0 + f_8^0)]$$

Recall that in the derivation, it is assumed that $f_1^0, f_3^0, f_4^0, f_7^0, f_8^0$ follow the rules (8), the equilibrium distribution at $j = 0$ is calculated using velocity (u_0, v_0), and f_2^0, f_5^0, f_6^0 depend on the boundary condition implemented.

Obviously, the vertical velocity in the interior of the flow domain may not equal the injection velocity if a boundary condition does not satisfy $\tilde{v}_0 = v_0$. The interior vertical velocity can be obtained by solving the quadratic equation (29).

As to the slip velocity, by comparing Eq. (26) with Eq. (28), we have

$$U_s^0 = \frac{12(\tau - 1)}{2\tau - 1} \frac{\tilde{u}_0 - u_0}{2 + R_b} \tag{30}$$

where $R_b = v_b \delta_x/\nu$. The same result can be obtained at the top boundary:

$$U_s'' = \frac{12(\tau - 1)}{2\tau - 1} \frac{\tilde{u}_n - u_n}{2 - R_b} \tag{31}$$

With the above results, we can explicitly analyze the different schemes for hydrodynamic boundary condition.

1. *Equilibrium scheme.* For a boundary condition with nonzero velocity, the bounce-back scheme is obviously not valid. A common practice in the LBE simulation is to assign the corresponding equilibrium distribution to the distribution functions at a boundary node. In our case, applying this scheme at the bottom boundary gives

$$f_2^0 = \frac{\rho}{9}\left[1 + 3\frac{v_0}{c} + 3\frac{v_0^2}{c^2} - \frac{3}{2}\frac{u_0^2}{c^2} \right]$$

$$f_5^0 = \frac{\rho}{36}\left[1 + 3\frac{u_0}{c} + 3\frac{v_0}{c} + 3\frac{u_0^2}{c^2} + 3\frac{v_0^2}{c^2} + 9\frac{u_0 v_0}{c^2} \right]$$

$$f_6^0 = \frac{\rho}{36}\left[1 - 3\frac{u_0}{c} + 3\frac{v_0}{c} + 3\frac{u_0^2}{c^2} + 3\frac{v_0^2}{c^2} - 9\frac{u_0 v_0}{c^2} \right]$$

Notice that assigning the equilibrium distribution to f_1^0, f_3^0 is consistent with Eqs. (8), and the values of f_4^0, f_7^0, f_8^0 are irrelevant to the flow inside. Here we use f_4^0, f_7^0, f_8^0 as given in Eqs. (8), so that Eqs. (28) and (29) are still valid for a simpler presentation. With this information, it is easy to derive

$$\tilde{v}_0 - v_0 = \frac{1}{2\tau}\left(v_0 - v_1 + \frac{v_0^2 - v_1^2}{c} \right) + (v_1 - v_0) \tag{32}$$

Substitution of this into Eq. (29) leads to $v_1 = v_0$, and thereafter, $v_j = v_b, \forall j$.
In the horizontal direction, it is easy to prove

$$U_s^0 = \left(1 - \frac{1}{\tau} \right)\frac{2 - R}{2 + R}(u_1 - u_0)$$

and similarly at the top boundary

$$U_s^n = \left(1 - \frac{1}{\tau} \right)\frac{2 + R}{2 - R}(u_{n-1} - u_n)$$

Substituting Eq. (26) with $j = 1$ and $j = n - 1$ into above two equations, we can obtain the final explicit expression for the slip velocities:

$$U_s^0 = -\frac{(\tau - 1)(\lambda - 1)(\tau\lambda - \tau - \lambda)}{\lambda^n(\tau\lambda - \tau + 1) + \lambda(\tau\lambda - \tau - \lambda)}(u_n - u_0) \tag{33}$$

$$U_s^n = \frac{(\tau - 1)(\lambda - 1)\lambda^n(\tau\lambda - \tau + 1)}{\lambda^n(\tau\lambda - \tau + 1) + \lambda(\tau\lambda - \tau - \lambda)}(u_n - u_0) \tag{34}$$

Obviously, the equilibrium scheme generally yields a nonzero slip velocity.
Let $\delta_x \to 0$; it is easy to prove

$$U_s^0 \sim \frac{1}{n}, \qquad U_s'' \sim \frac{1}{n}$$

This states that the slip velocity is of first order in space.

2. *Nonslip schemes.* With the nonslip schemes in refs. 2 and 3 we
have

$$\tilde{u}_0 = u_0, \qquad \tilde{v}_0 = v_0, \qquad \tilde{u}_n = u_n, \qquad \tilde{v}_n = v_n \tag{35}$$

Obviously, this boundary condition yields a zero slip velocity and hence
the boundary condition can be implemented correctly.

We also carried out numerical simulations for the Couette flow with
injection at boundaries. The system is exactly the same as the one used in
simulations for the Poiseuille flow, i.e., $N_x \times N_y = 16 \times 4$. The bottom wall
is fixed and the top wall moves at a speed of $0.1c$. For consistency, we
adjusted the value of the vertical injection velocity to yield the same
Reynolds number $Re = v_h L / v$.

Figure 4 shows the velocity profile for $Re = 2.0$ with different values of τ.
The theoretical solutions of the Navier–Stokes equation are also included
for comparison. The results with the equilibrium scheme yield a nonzero
slip velocity as long as $\tau \neq 1$, while the schemes in refs. 2 and 3 yield a zero
slip velocity regardless of the value of τ. All the numerical results coincide
with our analytical solution. Figure 5 shows the slip velocity for $Re = 1.0$
with the equilibrium scheme as a function of τ. Again, the numerical results
agree excellently with our analytic results.

2.3. Slip Velocity and Momentum Exchange

Another interesting phenomenon we found is that the slip velocity is
highly related to the momentum exchange at boundaries. Let us introduce
the quantity

$$\Delta M = \frac{cV}{\delta_t A} \left[(f_5^1 - f_6^1) - (f_8^0 - f_7^0) \right] \tag{36}$$

where V is the volume of the unit cell and A is the surface area between
two adjacent cells through which the momentum is transferred. In the 2D
nine-bit model, $V = \delta_x^2$ and $A = \delta_x$. The physical significance of ΔM is very
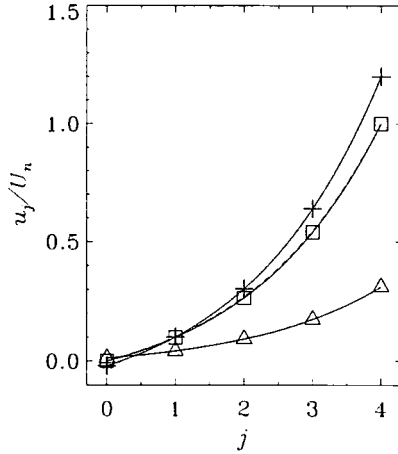
Fig. 4. The normalized velocity profile of the Couette flow with $Re = 2.0$. Dashed line, theoretical solution of the Navier–Stokes equation; solid lines, our analytic results with two types of boundary conditions and different values of r. ($\square$) The numerical results of lattice BGK simulation with the schemes in refs. 2 and 3; ($+$) the numerical results with the equilibrium scheme and with $\tau = 0.75$; ($\triangle$) the results with the equilibrium scheme and with $\tau = 2.0$.
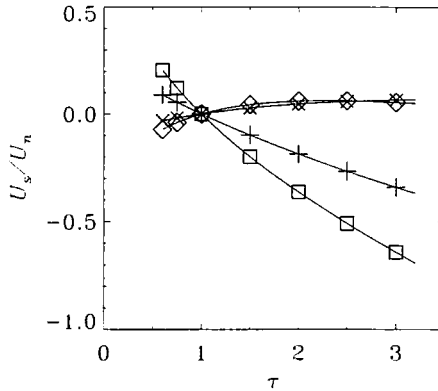

Fig. 5. The normalized slip velocity ($Re = 1.0$) of the Couette flow as a function of τ and the number of nodes across the channel, n, with the equilibrium scheme. Solid lines, our analytic results. ($\square$, $+$) The slip velocity in numerical simulations at the top wall and with $n = 4$ and 8, respectively; ($\diamond$, $\times$) the slip velocity in numerical simulations at the bottom wall and with $n = 4$ and 8, respectively.

clear: ΔM is the net tangential momentum exchange per time step and per unit area across the middle surface between the wall layer and the first flow layer. It can be shown that the slip velocity along the wall U_s is a direct consequence of inadequate momentum dissipation. For the Poiseuille flow, we have

$$\Delta M = c^2[(f_5^1 - f_6^1) - (f_8^0 - f_7^0)]$$

$$= \left(1 - \frac{1}{\tau}\right) c^2[f_5^0 - f_6^0] - c^2[f_8^0 - f_7^0] + \frac{c}{6\tau}\rho u_0 + \frac{c}{6}\delta_t \rho G$$

$$= c^2[f_5^1 - f_6^1] - \left(1 - \frac{1}{\tau}\right) c^2[f_8^1 - f_7^1] - \frac{c}{6\tau}\rho u_1 - \frac{c}{6}\delta_t \rho G$$

Addition of the last two equations gives

$$2\Delta M = \left(2 - \frac{1}{\tau}\right) \Delta M - \frac{c}{6}\left(2 - \frac{1}{\tau}\right) \rho(u_1 - u_0) + \left(1 - \frac{1}{\tau}\right) \rho c(\tilde{u}_0 - u_0) \quad (37)$$

or

$$\Delta M = -\rho \nu \frac{u_1 - u_0}{\delta_x} + (\tau - 1)\, \rho c(\tilde{u}_0 - u_0) \quad (38)$$

Recall that the slip velocity

$$U_s = \frac{6(\tau - 1)}{2\tau - 1}(\tilde{u}_0 - u_0)$$

Thus, keeping the slip velocity to be zero for an arbitrary τ is equivalent to having

$$\Delta M = -\rho \nu \frac{\partial u}{\partial y}\bigg|_{j = 1/2}$$

provided the derivative is second-order accurate in δ_x. In other words, the momentum dissipation by the wall must be equal to the stress applied by the fluid at the middle of the wall layer and the first flow layer.

A similar momentum exchange can be found for the Couette flow with vertical injection:

$$\Delta M = -\rho \nu \frac{u_1 - u_0}{\delta_x} + \frac{\rho}{2}(u_1 + u_0)\, v + (\tau - 1)\, \rho c(\tilde{u}_0 - u_0) \quad (39)$$

Again, a zero slip velocity implies that the momentum dissipation by the wall is equal to the momentum transfer carried by the vertical velocity plus the stress applied by the fluid (evaluated at the middle of the wall layer and first flow layer).

2.4. Bounce Back with Halfway Wall

In the previous subsections, the bounce-back boundary condition has been shown to yield a nonzero, first-order slip velocity at the bounce-back row for the Poiseuille and Couette flows. On the other hand, the bounce-back boundary condition has its own merit: easy implementation, which has been considered as one of the advantages of LGA and LBE. Although being attractive, the new boundary conditions proposed in refs. 1–3 have difficulties in implementation for a complex geometry like that in porous media, in which boundaries usually do not orient in either x or y direction. Besides, some additional considerations are needed for corner nodes. If a "complete" bounce-back rule, with every distribution simply reversing its direction, can work with a halfway wall, it will be very useful in practice. By a "halfway wall" we mean a wall placed at halfway between the bounce-back row and the first flow row.

For a stationary wall, it has been proved that the bounce-back boundary condition with the halfway wall has a second-order accuracy for some simple flows in the cases of FHP LGA[15] and LCHC LBE[16] for a suitable choice of the second eigenvalue of the collision matrix. This linear analysis was of the first order in gradient in ref. 15 and second order in ref. 16. In ref. 18 the theoretical result of Poiseuille flow with the square forcing[21] (equivalent to bounce-back boundary condition with a halfway wall) for FHP LBGK indicates a second order of accuracy. Using the results presented in previous subsections, we can prove that the bounce-back boundary condition with halfway wall is of second-order accuracy for the present LBGK models for the stationary walls of the simple flows considered. We will also give the explicit expression for the slip velocity.

First let us consider the bounce-back with halfway wall for the Poiseuille flow. The setup of the system is a little different from previous subsections. Nodes with $j = 1,..., n - 1$ are inside the flow and nodes $j = 0$, n are the bounce-back rows. After a complete bounce back, we have $f_2^1 = f_4^0$, $f_5^1 = f_7^0$, $f_6^1 = f_8^0$; the exchange of f_1^0 with f_3^0 has no effect on the flow. The walls are located at $j = 1/2$, $j = n - 1/2$. The evolution equation is the same as given in Eq. (1), but the width of the channel now becomes $L = (n - 1) \delta_x$ instead of $L = n\delta_x$. It has been previously (in Section 2.1) shown that with the bounce-back boundary condition at both bottom and

top walls, the velocity profile of the LBGK model for the Poiseuille flow
[Eqs. (15) and (20)] is

$$u_j = \frac{3G\delta_t}{2\tau - 1} j(n-j) + \frac{G\delta_t}{2(2\tau - 1)\, n^2} \left[(2\tau - 1)(4\tau - 3) - 3n\right] \qquad (40)$$

For the setup of halfway wall, the forcing G is related to the exact central
velocity $\bar{U}_c$ by $\bar{U}_c = L^2 G/8\nu$, where $L = (n-1)\,\delta_x$ is the width of the chan-
nel in this setup. Using $\bar{U}_c$, we find the velocity of the LBGK model for
Poiseuille flow:

$$u_j = \frac{4\bar{U}_c}{(n-1)^2} j(n-j) + \frac{2\bar{U}_c[(2\tau - 1)(4\tau - 3) - 3n)]}{3(n-1)^2} \qquad (41)$$

The exact solution of Poiseuille flow is

$$u_j' = \frac{\bar{U}_c(2j-1)(2n-2j-1)}{(n-1)^2} \qquad (42)$$

Thus, the error of the velocity from LBGK simulation is given by

$$u_j - u_j' = \frac{\bar{U}_c[4\tau(4\tau - 5) + 3]}{3(n-1)^2} \qquad (43)$$

While the error of velocity at the bounce-back row $j = 0$ is $O(1/(n-1))$,
indicating a first-order accuracy, the velocity inside the flow has a uniform
error $O(1/(n-1)^2)$, indicating a second-order accuracy for a fixed τ. There
is no need to adjust parameters in the model. Notice that for a fixed lattice
size, the error goes to infinity as $\tau \to \infty$. The conclusion is the same for the
FHP LBGK model.[18] For practical purposes, there is no need to take a
large value of τ in a simulation. In fact, the factor $4\tau(4\tau - 5) + 3$ in the
error expression has a maximal absolute value of only 3.25 for
$0.5 < \tau \leqslant 1.25$. Hence the bounceback with halfway wall is an acceptable
boundary condition for the Poiseuille flow. It is also noted that in this
bounce back, f_1^0 and f_3^0 can be interchanged (a complete bounce back)
without having any effect on the flow. Thus, the boundary condition is
implemented in a very simple way without distinguishing flow directions
and other directions.

Next let us consider the bounce back with halfway wall at the bottom
for the Couette flow with zero injection velocity. We will not change the
flow setup at the top wall and use a correct boundary condition like that

in refs. 2 and 3 there. After some algebraic manipulations we obtain the following x velocity:

$$u_j = U - \frac{2(n-j)}{2n-1} U = \frac{2j-1}{2n-1} U \tag{44}$$

where U is the velocity at the top. While the velocity at the bounce-back row ($j = 0$) is $O(1/(n-1))$, indicating a first-order accuracy, the velocity at the halfway wall ($j = 1/2$) is exactly zero, indicating that the result is the exact solution! These results also hold for the FHP LBGK model as given in the Appendix. Hence the bounce back with halfway wall deserves more attention in further simulations.

3. CONCLUSION AND DISCUSSION

In this paper, we have solved the lattice Boltzmann BGK equation for two simple flows under different boundary conditions. The solutions are verified by independent numerical simulations. Using these solutions, we further analyzed different schemes for implementation of the velocity boundary condition. We found that the schemes proposed in refs 1–3 give the zero slip velocity for the cases considered, and therefore are of second-order accuracy in space. Other schemes, such as bounce-back, equilibrium, etc., are only of first-order accuracy in general. The bounce-back scheme with halfway wall, however, is of second-order accuracy for the flows considered. Another interesting phenomenon we found is that the slip velocity is highly related to the momentum exchange at boundaries. A boundary condition is correct only when the momentum dissipation by the boundary is equal to the stress of the fluid. We hope this work can provide some help for future studies of boundary conditions. Needless to say, our analysis is only carried out for the 2D Poiseuille flow and the 2D Couette flow with injection at the boundaries. The analytical solutions for these flows are still too simple to use as general guidance for the boundary condition analysis. Further studies on more complicated flows are necessary.

APPENDIX. RESULTS FOR FHP LBGK MODEL

For the steady Poiseuille flow, the seven-bit BGK model on a triangular lattice (FHP LBGK model) with $\mathbf{e}_0 = 0$ and $\mathbf{e}_\alpha = [\cos((\alpha-1)\pi/3), \sin((\alpha-1)\pi/3)]\,c$, $\alpha = 1,...,6$, can be reduced as the following recursion forms:

$$f_0^j = \rho \left[r - \left(\frac{u_j}{c} \right)^2 \right]$$

$$f_1^j = \frac{1}{6} \rho \left[(1 - r) + 2 \frac{u_j}{c} + 3 \left(\frac{u_j}{c} \right)^2 \right] + \frac{\delta_x}{4c^2} \tau \rho G$$

$$f_2^j = \frac{1}{6\tau} \rho \left[6(1 - r) + \frac{u_{j-1}}{c} \right] + \left(1 - \frac{1}{\tau} \right) f_2^{j-1} + \frac{\delta_x}{4c^2} \rho G$$

$$f_3^j = \frac{1}{6\tau} \rho \left[6(1 - r) - \frac{u_{j-1}}{c} \right] + \left(1 - \frac{1}{\tau} \right) f_3^{j-1} - \frac{\delta_x}{4c^2} \rho G \qquad (A1)$$

$$f_4^j = \frac{1}{6} \rho \left[(1 - r) - 2 \frac{u_j}{c} + 3 \left(\frac{u_j}{c} \right)^2 \right] - \frac{\delta_x}{4c^2} \tau \rho G$$

$$f_5^j = \frac{1}{6\tau} \rho \left[6(1 - r) - \frac{u_{j+1}}{c} \right] + \left(1 - \frac{1}{\tau} \right) f_5^{j+1} - \frac{\delta_x}{4c^2} \rho G$$

$$f_6^j = \frac{1}{6\tau} \rho \left[6(1 - r) + \frac{u_{j+1}}{c} \right] + \left(1 - \frac{1}{\tau} \right) f_6^{j+1} + \frac{\delta_x}{4c^2} \rho G$$

where r is the fraction of rest particle mass density out of the total mass density; it can be adjusted between 0 and 1. The body force $\mathbf{F}$, with amplitude $\|\mathbf{F}\| = \rho G$, is along the direction of $\mathbf{e}_1$. The system satisfies the Navier–Stokes equation (6) with the kinetic viscosity

$$\nu = \frac{(2\tau - 1)}{8} \frac{\delta_x^2}{\delta_t} \qquad (A2)$$

and the speed of sound

$$c_s = \sqrt{\frac{1 - r}{2}} \, c \qquad (A3)$$

Inside the flow domain, it is easy to derive the same solution for u as in the square-lattice case:

$$u_j = \frac{4U_c j(n - j)}{n^2} + U_s$$

where $U_c = L^2 G / 8\nu$ is the central velocity as before. $L = n\delta_y$, with $\delta_y = \sqrt{3}\delta_x/2$ being the vertical distance between two adjacent lattice lines.

The slip velocity U_s depends on the boundary condition. The boundary conditions in refs. 1 and 3 generate a zero slip velocity, hence give the exact solution of the Poiseuille flow.

With the bounce-back boundary condition, for example, at the bottom, $f_2^1 = f_5^0$, $f_3^1 = f_6^0$, the slip velocity can be derived as

$$U_s = -\frac{2U_c(n+1)}{n^2} + \frac{3(2\tau^2 - 3\tau + 2)}{2(2\tau - 1)}\delta_t G \tag{A4}$$

which is of first order in general.

Similarly, for the case of bounce back with halfway wall, the error of the velocity of the LBGK is derived as

$$u_j - u_j' = \frac{\bar{U}_c(4\tau^2 - 6\tau + 1)}{(n-1)^2} \tag{A5}$$

the same result as in ref. 18, which is of second-order accuracy. The factor $4\tau^2 - 6\tau + 1$ takes a maximal absolute value of 1.25 for $0.5 < \tau \leqslant 1.25$. Notice also that a complete bounce back can be used for the bounce back with a halfway wall.

For the Couette flow with $v = 0$, the model at the beginning of this appendix can be used with $G = 0$. Suppose that we use a correct boundary condition as in refs. 2 and 3 at the top wall and use bounce back at the bottom; then the x velocity is

$$u_j = U - \frac{2(n-j)}{2n-1}U = \frac{2j-1}{2n-1}U \tag{A6}$$

where U is the velocity at the top. This is the same result as in the square-lattice case, and bounce back with halfway wall still gives the exact solution.

Other boundary conditions can be studied as well.

REFERENCES

1. D. R. Noble, S. Chen, J. G. Georgiadis, and R. O. Buckius, A consistent hydrodynamics boundary condition for the lattice Boltzmann method, *Phys. Fluids* **7**:203 (1995).
2. D. R. Noble, J. G. Georgiadis, and R. O. Buckius, Direct assessment of lattice Boltzmann hydrodynamics and boundary conditions for recirculating flows, *J. Stat. Phys.* **81**:17 (1995).
3. T. Inamuro, M. Yoshino, and F. Ogino, A non-slip boundary condition for lattice Boltzmann simulations, *Phys. Fluids* **7**:2928 (1995); Erratum, **8**:1124 (1996).
4. G. McNamara and G. Zanetti, Use of the Boltzmann equation to simulate lattice-gas automata, *Phys. Rev. Lett.* **61**:2332 (1988).

5. F. Higuera and J. Jimenez, Boltzmann approach to lattice gas simulations, *Europhys. Lett.* **9**:663 (1989).
6. H. Chen, S. Chen, and W. H. Matthaeus, Recovery of the Navier–Stokes equations using a lattice Boltzmann method, *Phys. Rev. A* **45**:R5339 (1991).
7. Y. H. Qian, D. d'Humières, and P. Lallemand, Lattice BGK models for the Navier–Stokes equation, *Europhys. Lett.* **17**:479 (1992).
8. R. Benzi, S. Succi, and M. Vergassola, The lattice Boltzmann equation: Theory and applications, *Phys. Rep.* **222**:145 (1992).
9. X. Shan and H. Chen, Lattice Boltzmann model for simulating flows with multiple phases and components, *Phys. Rev. E* **47**:1815 (1993); Simulation of non-ideal gases and liquid-gas phase transitions by the lattice Boltzmann equation, *Phys. Rev. E* **49**:2941 (1994).
10. A. J. C. Ladd, Numerical simulations of particulate suspensions via a discretized Boltzmann equation. Part I. Theoretical foundation, *J. Fluid Mech.* **271**:285 (1994); Numerical simulations of particulate suspensions via a discretized Boltzmann equation. Part II. Numerical results, *J. Fluid Mech.* **271**:311 (1994).
11. S. Chen, H. Chen, and W. H. Matthaeus, Lattice Boltzmann magnetohydrodynamics, *Phys. Rev. Lett.* **67**:3776 (1991).
12. S. P. Dawson, S. Chen, and G. Doolen, Lattice Boltzmann computations for reaction-diffusion equations, *J. Chem. Phys.* **98**:1514 (1993).
13. S. Hou, Q. Zou, S. Chen, G. D. Doolen, and A. Cogley, Simulation of cavity flow by the lattice Boltzmann method, *J. Comp. Phys.* **118**:329 (1995).
14. P. A. Skordos, Initial and boundary conditions for the lattice Boltzmann method, *Phys. Rev. E* **48**:4823 (1993).
15. R. Cornubert, D. d'Humières, and D. Levermore, A Knudsen layer theory for lattice gases, *Physica D* **47**(6):241 (1991).
16. I. Ginzbourg and P. M. Adler, Boundary condition analysis for the three-dimensional lattice Boltzmann model, *J. Phys. II France* **4**:191 (1994).
17. L.-S. Luo, H. Chen, S. Chen, G. D. Doolen, and Y.-C. Lee, Generalized hydrodynamic transport in lattice-gas automata, *Phys. Rev. A* **43**:R7097 (1991).
18. Q. Zou, S. Hou, and G. D. Doolen, Analytical solutions of the lattice Boltzmann BGK model, *J. Stat. Phys.* **81**:319 (1995).
19. U. Frisch, D. d'Humières, B. Hasslacher, P. Lallemand, Y. Pomeau, and J.-P. Rivet, Lattice gas hydrodynamics in two or three dimensions, *Complex Systems* **1**:649 (1987).
20. A. K. Gunstensen and D. H. Rothman, Microscopic modeling of immiscible fluids in three dimensions by a lattice-Boltzmann method, MIT Porous Flow Project, Report No. 4, 20 (1991).
21. L. P. Kadanoff, G. R. McNamara, and G. Zanetti, From automata to fluid flow: Comparisons of simulation and theory, *Phys. Rev. A* **40**:4527 (1989).